

Optical discrete solitons in waveguide arrays.

2. Dynamic properties

Ulf Peschel,* Roberto Morandotti, John M. Arnold, and J. Stewart Aitchison†

Department of Electronics and Electrical Engineering, University of Glasgow, Glasgow G12 8QQ, Scotland, UK

Hagai S. Eisenberg and Yaron Silberberg

Department of Physics of Complex Systems, Weizmann Institute of Science, 76100 Rehovot, Israel

Thomas Pertsch and Falk Lederer

Physikalisch-Astronomische Fakultät, Friedrich-Schiller Universität Jena, Jena 07743, Germany

Received October 31, 2001; revised manuscript received June 12, 2002

An AlGaAs waveguide array below the half-bandgap is used to investigate experimentally basic dynamic features of discrete systems. In particular, nonlinear locking of a discrete soliton to its input waveguide was observed for certain input conditions. We also investigated the soliton dynamics as a function of the position of the initial excitation and found that small shifts from the centers of symmetries of the structure could be greatly enhanced. Both effects depend on the geometry of the array and on the beam size. © 2002 Optical Society of America

OCIS codes: 190.0190, 190.4390, 190.4420.

1. INTRODUCTION

A fascinating feature of intense light beams is their ability to self-trap by creating their own waveguide. Spatial solitons originate from a balance between material nonlinearity and diffraction and can be easily generated in bulk materials¹ or in planar waveguides,² where the slab confines one of the spatial dimensions. By imposing a phase gradient on the input beam, one can steer solitons into a desired direction, a property that can be used to route and to switch signals in optical fiber networks. The existence of spatial solitons has also been predicted for an infinite array of identical, weakly coupled waveguides in Ref. 3. In such a structure, when low intensity light is injected into either one or just a few waveguides, it will couple and spread to an increasing number of waveguides as it propagates, broadening its spatial distribution through discrete diffraction. By injecting a strong optical field into a single waveguide, it is possible for one to modify its refractive index through the optical nonlinearity of the material and to decouple the waveguide from the rest of the array. It has been shown experimentally that, even when light is coupled to more than one waveguide, it can propagate while keeping a fixed spatial profile.⁴ Similar localized waves are found in many areas of physics. They are known as discrete solitons and appear on nonlinear lattices of various physical origin³ (for an overview see Ref. 5 and the references therein). Here we describe several experimental studies of the dynamic properties exhibited by discrete solitons. In particular, we investigated experimentally and numerically the effect of beam size, power level, and geometry of the structure on the properties of optical discrete solitons. In agreement with earlier theoretical predictions^{6–8} and ini-

tial experimental observations,⁹ we observed power-induced locking of initially tilted beams and position-induced soliton steering.

The paper is structured as follows. First we review a few basic properties of discrete solitons that are essential for understanding the experimental results. Then we describe the experimental setup, the methods of measurement, and the way we modeled the experiments. A short summary concludes the paper.

2. GENERAL PROPERTIES OF DISCRETE SOLITONS

We start with a brief description of some basic properties of discrete solitons. Consider an infinite array of single-mode waveguides that are weakly coupled through their evanescent field. We assume that the modes of the individual waveguides remain unchanged and that only the mode amplitudes E_n evolve during propagation.¹⁰ In an ideal case, where no losses are present and the excitation has no time dependence (continuous-wave excitation), the field evolution is described by the discrete nonlinear Schrödinger (DNLS) equation³:

$$i \frac{dE_n}{dz} + C(E_{n+1} + E_{n-1}) + \gamma |E_n|^2 E_n = 0, \quad (1)$$

where C is the coupling coefficient and γ is the nonlinear parameter that accounts for the optical Kerr effect. In fact, a model based on Eq. (1) reproduces qualitatively most of the effects observed quite well, even when it fails sometimes to produce good quantitative agreement with

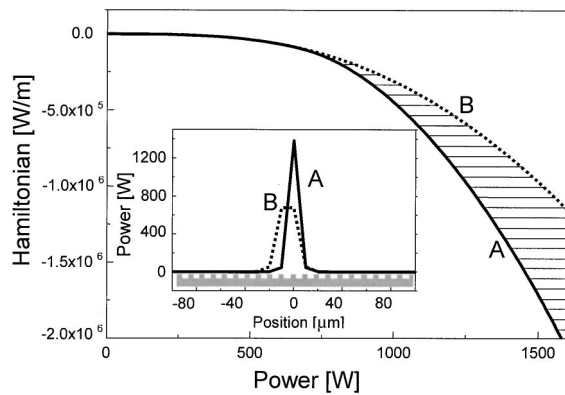


Fig. 1. Hamiltonian versus energy for a type A (centered on a guide) and a type B (centered between two guides) solution. The difference marks the PNP, which describes the dynamic properties of the solution. The inset shows the two types of solution for a peak power of approximately 1500 W.

the experimental results. We restrict most of the discussion to Eq. (1) and will use more involved techniques only if required.

The nonlinear term in Eq. (1) is significant only at high powers and can be ignored in the low-intensity regime, where the equation can be solved analytically.¹¹ This low-power linear solution describes discrete diffraction in an array of waveguides. When the input beam is injected into a single waveguide, a pronounced diffraction cone is obtained, where most of the power propagates in two wings (for experimental observations of this effect see Refs. 4 and 12). Spectral analysis of Eq. (1) shows that these wings are associated with propagation at zero spatial dispersion. Hence, for this particular angle of propagation the beam does not diffract up to second order, as was experimentally demonstrated in Refs. 13 and 14. Even when the power is increased the field never escapes from this cone. Since only approximately $4CL$ waveguides are excited after propagating a distance L , it is not necessary to fabricate wider arrays.

If we restrict our study to consider fields that vary slowly across the array, the DNLS equation appears as a natural discretization of the well-known nonlinear Schrödinger equation. However, even though the latter is integrable,¹⁵ the behavior of the DNLS equation must be described in terms of approximate analytical solutions or through numerical methods.¹⁶ Two limiting cases that allow for an analytical description can be defined. The first, also known as the long-wavelength limit, can be described by the continuum approximation that leads to the nonlinear Schrödinger equation and generates similar solutions.¹⁵ These solitons are able to move in the array almost undisturbed. In the second case the excitation is localized mostly in a single waveguide, which is effectively decoupled from the rest of the array.⁸ In this limit the mutual interaction and any energy transport between the guides are blocked by the nonlinearity. The experiments reported in this paper describe an intermediate situation in which both transverse propagation and locking could occur.

Two types of soliton can propagate parallel to the waveguide direction (with no transverse motion). They can be either centered directly on or exactly between two wave-

guides, which we refer to as type A and type B solutions, respectively. To formulate the dynamics of the solitons we introduced two conserved quantities of the DNLS equation, total guided power P and Hamiltonian H :

$$P = \sum_n |E_n|^2,$$

$$H = \sum_n \left(C|E_n - E_{n-1}|^2 - \frac{\gamma}{2}|E_n|^4 \right). \quad (2)$$

For a given power level the type A marks a minimum of the respective Hamiltonian (see Fig. 1), which corresponds to a stable solution. In contrast the type B solution has a higher value and is unstable. The difference between the Hamiltonian of the solutions, the so-called Peierls–Nabarro potential (PNP), grows with increasing power and localization, marking the influence of discreteness. A localized solution, which is forced to move, is sometimes centered on a guide and sometimes between two waveguides. During the solution's transverse propagation, it must overcome the PNP while crossing a guide. Hence the PNP is relevant to the dynamic properties of the system.

3. EXPERIMENTAL REALIZATION AND MODELING

The sample used for the measurements (see Fig. 2) was an array of 41 waveguides etched $0.9 \mu\text{m}$ in the cladding of an AlGaAs slab, which was composed of a core of $\text{Al}_{0.18}\text{Ga}_{0.82}\text{As}$, $1.5 \mu\text{m}$ thick, sandwiched between two cladding layers of $\text{Al}_{0.24}\text{Ga}_{0.76}\text{As}$. The upper and the lower layers were 1.5 and $4.0 \mu\text{m}$ thick, respectively. These dimensions were chosen to guarantee single-mode operation. The $4\text{-}\mu\text{m}$ -wide waveguides had a center-to-center distance of $9 \mu\text{m}$. The sample was 6 mm long. The experimental setup is depicted in Fig. 2 together with a micrograph of the array. The laser source was a Spectra-Physics Tsunami-Opal optical parametric oscillator, with an emission wavelength of 1530 nm , a pulse length of approximately 130 fs , and a repetition rate of 80 MHz . This wavelength, below half-bandgap of the material, was chosen to minimize the detrimental effects of nonlinear absorption. The input beam that was

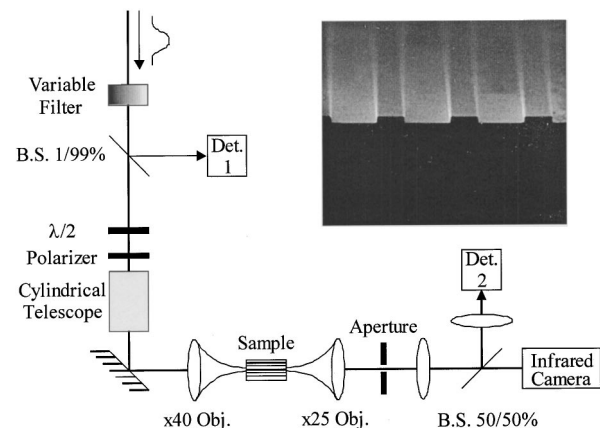


Fig. 2. Experimental setup and a viewgraph of the sample.

launched into the sample was elliptically shaped, TE polarized with a fixed height of $3\ \mu\text{m}$, but with three different widths equal to 9, 13, and $20\ \mu\text{m}$, respectively. The field at the output facet was recorded with an infrared camera. To gain insight into the field evolution in the array we used numerical simulations. Although the DNLS equation [see Eq. (1)] allows for a basic understanding of the physics involved, accurate modeling of the experimental results requires the consideration of transient and absorptive effects. The resulting modification of Eq. (1) is

$$i \frac{\partial E_n}{\partial z} - \frac{D}{2} \frac{\partial^2 E_n}{\partial t^2} + i \frac{\alpha_1}{2} E_n + \gamma |E_n|^2 E_n + i \alpha_3 |E_n|^4 E_n + C(E_{n+1} + E_{n-1}) = 0, \quad (3)$$

where the parameters are the chromatic dispersion $D = 1350\ \text{ps}^2/\text{km}$, the linear losses $\alpha_1 = 0.9\ \text{cm}^{-1}$, the Kerr nonlinearity $\gamma = 3.6\ \text{m}^{-1}\text{W}^{-1}$, the three-photon absorption coefficient $\alpha_3 = 10^{-4}\ \text{m}^{-1}\text{W}^{-1}$, and the coupling term $C = 0.82\ \text{mm}^{-1}$. Except for the linear losses, we derived all these values from a calculation of the mode profiles and by using material constants published in the literature.¹⁷ We determined the linear losses, which are due mainly to scattering of imperfections, by evaluating the amplitude of the Fabry-Perot fringes in transmission experiment.

Although Eq. (1) gives a good qualitative explanation for most of our results, Eq. (3) could be used for a better quantitative analysis. In particular, Eq. (3) predicts higher power levels for most effects. This power increase is due not only to the losses included but also to the transient behavior of the pulse. Purely dispersive effects are somewhat weak. However, temporal effects are not entirely negligible because of the temporal profile of the pulses. The peak of the pulse will undergo nonlinear changes, whereas the front and the tail will not. Consequently, the expected nonlinear effects will be somewhat averaged and will appear slightly less pronounced than those predicted by continuous-wave simulations.

The excitation at the input facet is assumed to have a Gaussian profile, and the amplitude of the mode of the n th waveguide is

$$E_n(z = 0, t) = \frac{\sqrt{P_{\max}}}{\left\{ \sum_n \exp[-2(n - n_0)^2/W^2] \right\}^{1/2}} \times \exp[-(n - n_0)^2/W^2 - (t - t_0)^2/T^2], \quad (4)$$

where P_{\max} is the peak power, T is the pulse duration, and n_0 is the position of the center of the input beam and is not necessarily an integer. Effective spatial width W in units of spacing between neighboring guides d is determined by beam width W_b and by the mode diameter W_m (both full width at half-maximum). Assuming the mode to be Gaussian as well, we can approximate W to be

$$W \cong \left[\frac{W_b^2 + W_m^2}{2 \ln(2)d^2} \right]^{1/2}. \quad (5)$$

For a typical mode diameter of $W_m = 6\ \mu\text{m}$ (FWHM) and a waveguide spacing of $d = 9\ \mu\text{m}$, the three available beam widths ($W_b = 9, 13,$ and $20\ \mu\text{m}$ FWHM) correspond to effective diameters of the excitation of $W \approx 1.02, 1.55,$ and 1.97 , respectively. The input power was determined from the measured output power, after we evaluated the losses through Eq. (3). The coupling efficiency was between 10% and 20%.

4. EXPERIMENTAL RESULTS AND INTERPRETATIONS

A. Soliton Formation and Beam Breakup

We briefly discuss soliton formation in waveguide arrays. Depending on the power level and the beam width three different situations can occur (see Figs. 3 and 4). In the linear case the beam diffracts [Fig. 3(b) and area I in Fig. 4]. The narrower beams require higher power to form a discrete soliton [Fig. 3(c) and area II in Fig. 4]. If the beam is wide enough and therefore close to the continuous limit, it finally splits for the highest input power [Fig. 3(c) and area III in Fig. 4]. Almost the same breakup is experimentally observed in a comparable slab waveguide (unetched sample). The physics behind this effect can be interpreted in terms of the continuous limit, where this splitting is well known.¹⁸ However, in both cases, a two-soliton state of the nonlinear Schrödinger equation is

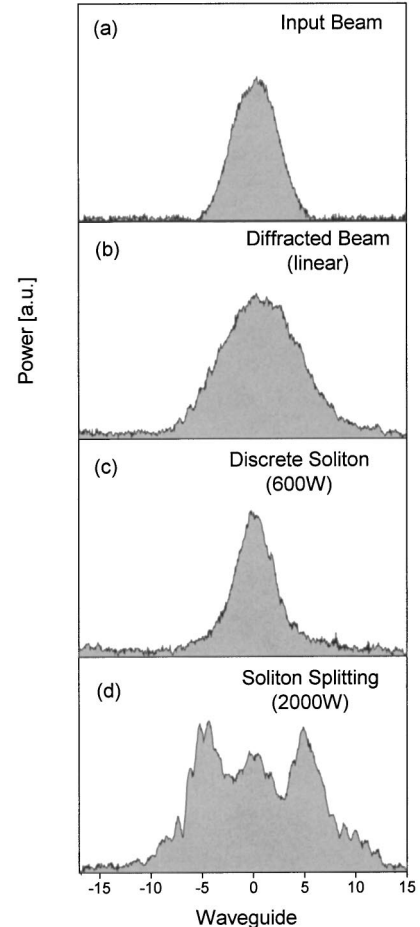


Fig. 3. Experimentally recorded soliton formation and beam breakup for a $20\text{-}\mu\text{m}$ -wide input beam and different power levels.

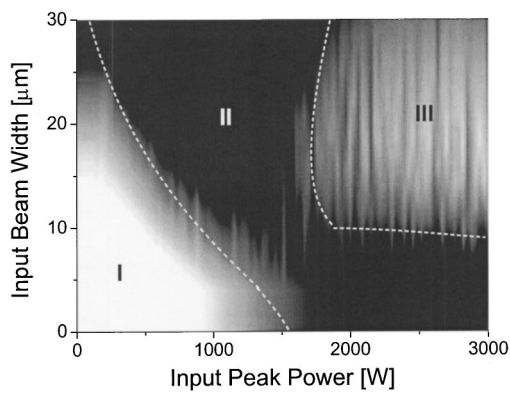


Fig. 4. Simulation of the width of the output field distribution on the basis of a complete model [see Eq. (3)] (white, wide output beam; black, narrow output beam). Depending on the beam size and the input power three different situations can be distinguished: I, linear diffractive spreading; II, formation of a discrete soliton; III, soliton splitting.

formed. Because it lacks binding energy, this bound state finally splits in the presence of nonlinear absorption,¹⁹ leading to novel physical behavior.

B. Experiments with Tilted Beams

The first group of experiments on dynamical effects was devoted to study lateral motion of discrete solitons following the tilting of the input wave front. A glass wedge was positioned in front of the input lens to generate a tunable phase tilt across the beam. In this way it was possible to vary the tilt angle of the wave front with respect to the input facet by up to 1 deg (angle inside the structure).

In Figs. 5 and 6 we show the output power distribution obtained with a narrow input beam (9 μm wide) launched along the array at two different angles. For low energy (top of Figs. 5 and 6) two wings can still be identified. Compared with a straight beam, these wings have considerably different power levels. Most of the input energy is translated by approximately 80 μm (eight or nine waveguides) from the original input position. We note that this translation is not increased for larger values of the input angle, but only the power imbalance between these two wings is increased (compare the tops of Figs. 5 and 6). As we discussed above, once the geometry of the array is fixed, the number of waveguides excited by the diffracting beam depends on the length of the sample but not on the input angle. This is markedly different from the continuous case in which an increased tilt leads to translational motion of the beam center. For small initial tilts the energy redistribution in the array is more pronounced than in a comparable slab waveguide. For example, considering the case of Fig. 4, the same tilted beam would have undergone a displacement of approximately 14 μm in a slab waveguide of the same length, whereas we observed a five times bigger shift in the array.

In a nonlinear case, the effects of discreteness are even more pronounced. Consider first the case of small input tilt (see Fig. 5). As we increase the power we observe how the light distribution, initially shifted away from the input waveguide, is relocated to the central position. This happens almost immediately once a discrete soliton is formed. However, this process depends critically on

the initial input angle. For larger tilts a soliton is formed but it continues to move sideways across the array. In this case, the soliton does not lock to the waveguide direction even at the highest input power. A question arises with regard to the maximum input angle that allows full locking of the initially moving soliton at the input wave-

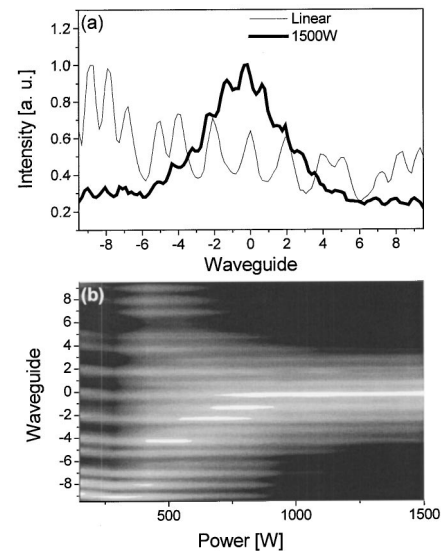


Fig. 5. Power-induced locking of a discrete soliton for a small initial tilt. (a) Field profiles for low (thin curve) and high (thick curve) power. (b) Contour plot of output field profiles versus input peak power (initial tilt, $\approx 0.15^\circ$ in AlGaAs; 9- μm beam size).

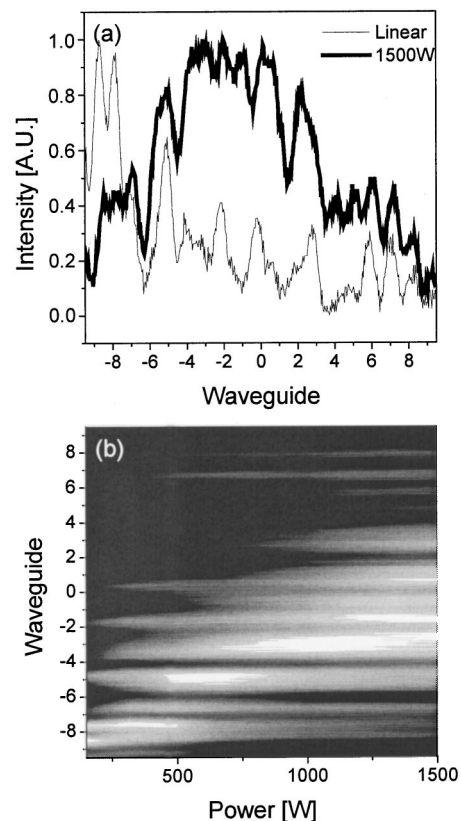


Fig. 6. Power-induced locking of a discrete soliton for a large initial tilt. (a) Field profiles for low (thin curve) and high (thick curve) power. (b) Contour plot of output field profiles versus input peak power (initial tilt, $\approx 0.5^\circ$ in AlGaAs; 9- μm beam size).

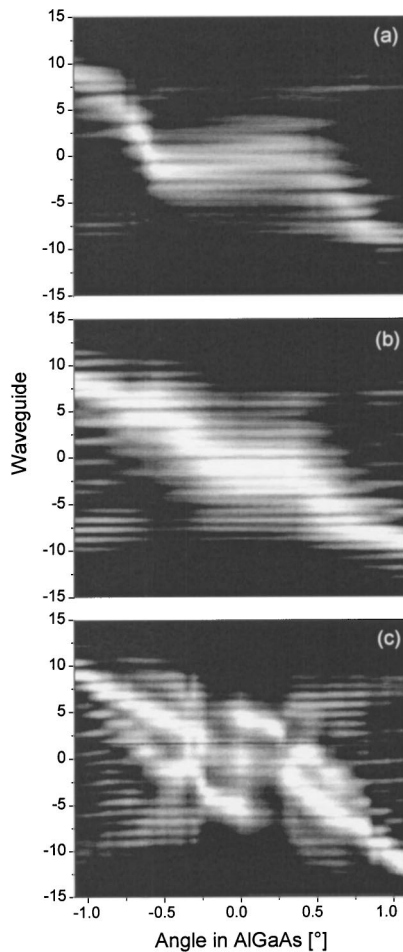


Fig. 7. Angular steering of a discrete soliton showing output profile versus input angle: (a) single soliton state with a narrow beam ($9\text{-}\mu\text{m}$ beam size, $\approx 1500\text{-W}$ peak power); (b) single soliton state with a wider beam ($13\text{-}\mu\text{m}$ beam size, $\approx 1200\text{-W}$ peak power); (c) soliton breakup for a larger beam ($20\text{-}\mu\text{m}$ beam size, $\approx 2000\text{-W}$ peak power).

guide. To study this particular point, we fixed the input power at the level necessary to generate a single soliton state for two specific beam sizes equal to 9 and $13\ \mu\text{m}$, respectively [see Figs. 7(a) and 7(b)]. We note that, for the narrowest beam size (when approximately two waveguides are excited), the effects of discreteness are stronger and locking is achieved over a larger range. The locking range of the soliton is clearly diminished for the second beam. To confirm this trend, we also generated a $20\text{-}\mu\text{m}$ -wide beam, which could overlap approximately three waveguides. No locking was observed in this case, suggesting that discreteness did not have any apparent effect.

The basic principle behind this locking behavior can be understood on the basis of the PNP discussed above (see Fig. 1). A moving soliton must conserve both its initial power and the Hamiltonian, while passing continuously between stable and unstable configurations with significantly different Hamiltonian values. The PNP is a measure of how much the beam must deviate from a stationary profile to be able to move. The phase tilt imposed on the input wave front can be regarded as an effective kinetic energy, giving the soliton translational momentum.

The more intense (and better-confined) soliton requires more kinetic energy and larger tilt to overcome the PNP.

Beam breakup that is due to the action of nonlinear absorption introduces some new features, which cannot be predicted on the basis of the DNLS equation. In this case, the initial tilt induces merely power redistribution between the two emerging beams. Only for larger tilts does the splitting disappear and a moving structure is formed [see Fig. 7(c)].

C. Experiments with Transversally Displaced Beams

Discreteness not only suppresses initial lateral motion, it can also generate an opposite effect, inducing the lateral acceleration of a beam launched along the waveguide direction. We investigated the sensitivity of discrete solitons to small horizontal translations. In this experiment we used an untilted, flat-phase input beam. After the beam was aligned at normal incidence, we translated the sample by using a piezodriven stage. The sample was moved laterally by a distance larger than the separation of two waveguides. We excited a fundamental soliton and scanned the beam $14\ \mu\text{m}$ across the input facet, corresponding to approximately 1.5 times the waveguide spacing. We verified that the overall coupling efficiency was practically independent of the spatial position of the excitation. Numerical analysis also confirmed that, even for the smallest beams ($9\ \mu\text{m}$), the energy loss during lateral translation is less than 10%. Two output field profiles are displayed in Fig. 8. A complete scan of different input positions and the resulting varying output profiles are presented in Fig. 9. Simulations based on Eq. (1) demonstrate that the induced beam tilt can be explained on the basis of the DNLS equation (see Fig. 10).

We note that, when we injected the soliton exactly into the center of a waveguide (solid line in Fig. 9, corresponding to a stable type A soliton) or into the middle between two waveguides (dashed line in Fig. 9, unstable type B soliton), the soliton propagates straight along the array because of the symmetry of this configuration.

We now discuss the results for the small input beam ($9\text{-}\mu\text{m}$ width FWHM). In this case, the overall displacement of the field at the output facet is as much as ten times larger than the initial shift of the input beam [see Fig. 9(a)]. The differential amplification of initial shifts is strongest when the excitation is exactly in the middle between two waveguides (dashed line in Fig. 9). In this

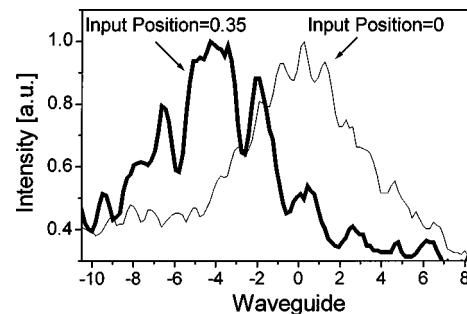


Fig. 8. Output field profiles for an input position on a waveguide (position 0) and between two waveguides (position $3.2\ \mu\text{m}$ or 0.35 waveguide spacing). The soliton moves in the direction opposite the displacement ($9\text{-}\mu\text{m}$ beam size, 1500-W peak power, no initial tilt was introduced).

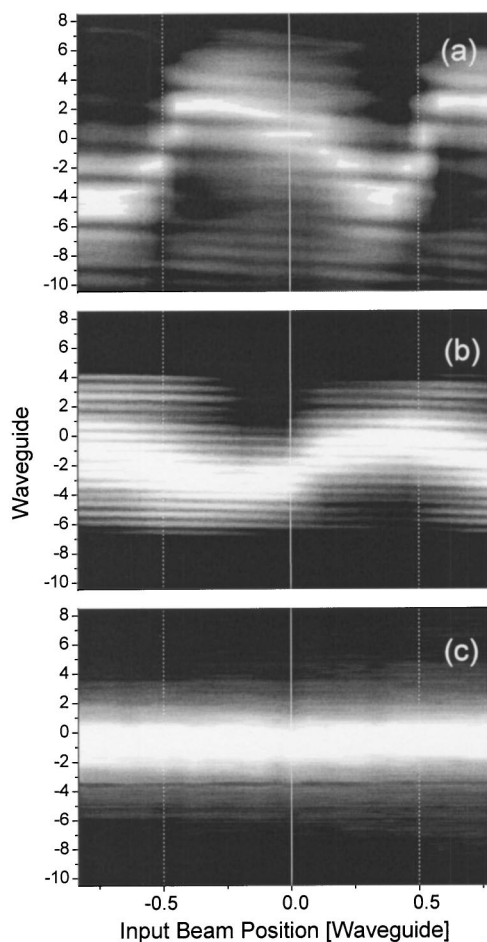


Fig. 9. Output field profiles versus input position for single soliton states of different widths: (a) 9- μm beam size, 1500-W peak power, (b) 13- μm beam size, 1200-W peak power, (c) 20- μm beam size, 800-W peak power (solid line, input beam centered on a waveguide; dashed line, input beam centered between two waveguides).

case, small variations of the input position cause the output field to scan as many as eight waveguides. The soliton state, which is excited for excitation between two waveguides, is unstable and small deviations induce its decay. In other words, any asymmetry between the power levels in the input waveguides results in a different nonlinear refractive index generated by the Kerr effect. Consequently, a tilt of the phase front is induced and energy is transferred toward the high intensity edge of the spatial profile. The phase tilt provides enough momentum to the motion, and also prevents the localization of the soliton. In the PNP picture, the simultaneous conservation of power and Hamiltonian dictates that the initial excess of the latter quantity for the unstable (type B) soliton is transformed into the kinetic energy required by the stable (type A) soliton to propagate across the array (see Fig. 1 and the two upper graphs in Fig. 10).

The effect of discreteness and the influence of the PNP diminish for larger beam sizes. To verify this fact we increased the beam size to 13 μm . We observed that, in the same experimental conditions, the amplification of the lateral translation was reduced from eight to approximately three waveguides [compare Figs. 9(a) and 9(b)].

A further increase in the beam size (up to 20 μm FWHM for the fundamental soliton) adequately suppressed any effect that is due to discreteness [see Fig. 9(c)]. The soliton is then insensitive to the different input positions and retains its straight propagation.

A more detailed numerical analysis of the DNLS equation [Eq. (1)] reveals that these effects can be observed only for input power levels slightly above the formation threshold for a discrete soliton (see Fig. 11). If the power is increased further, a soliton excited between two guides starts to move but eventually locks on the neighboring waveguide. Basically the increased PNP relocks the soliton. The excess Hamiltonian is now emitted through a certain amount of additional radiation. However, losses and transient effects seem to increase the mobility of the soliton in the real experiment. Even for higher initial pulse energies the soliton power constantly decreases during propagation and, consequently, the effective potential barrier diminishes. On the basis of the complete Eq. (3) we checked how this steering effect varies for different values of input powers and pulse widths (see Fig. 12). We determined that there is an optimum region around 1500 W that we have just hit with the initial conditions that correspond to Figs. 8 and 9(a). For a 9- μm beam but higher input power levels, the sensitivity of the system with respect to initial displacements is again diminished. Although the respective power levels are too low, this ten-

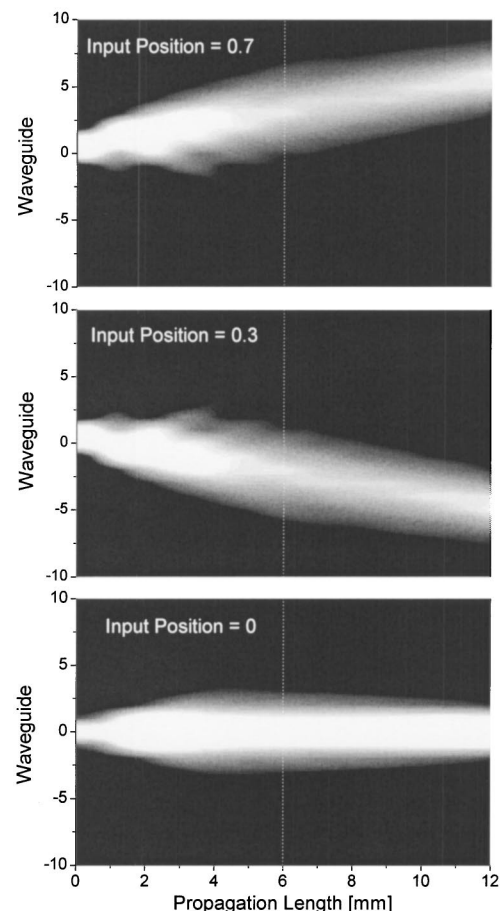


Fig. 10. Simulation of the field propagation based on the DNLS equation [see Eq. (1)] for different input positions (700-W power; 9- μm beam size; dashed line, sample length).

dependency is already predicted by the simulations based on the DNLS equation (see Fig. 11). In the parameter domain where single soliton states are excited, we found no other point of extreme sensitivity. However, when pulse breakup occurs, initial displacements are again amplified considerably (compare Figs. 4 and 12).

To confirm the above predictions we used the widest beam ($20\ \mu\text{m}$) and increased the power until soliton splitting occurred (see Fig. 13). When we translated the array the induced asymmetry caused the preferential transfer of energy in only one of the two beams generated by the decay of the broad soliton. Contrary to the experiments with a fundamental soliton we did not observe a motion but did observe an energy transfer between two channels defined by the soliton breakup. As before, the biggest change in the output position was observed for an almost infinitesimal displacement around the point of unstable equilibrium.

These novel results could be the bases of an all-optical interconnect in future communication systems. Piezoelectric transducers could be used to switch incoming signals. Alternatively, suitable power redistribution could

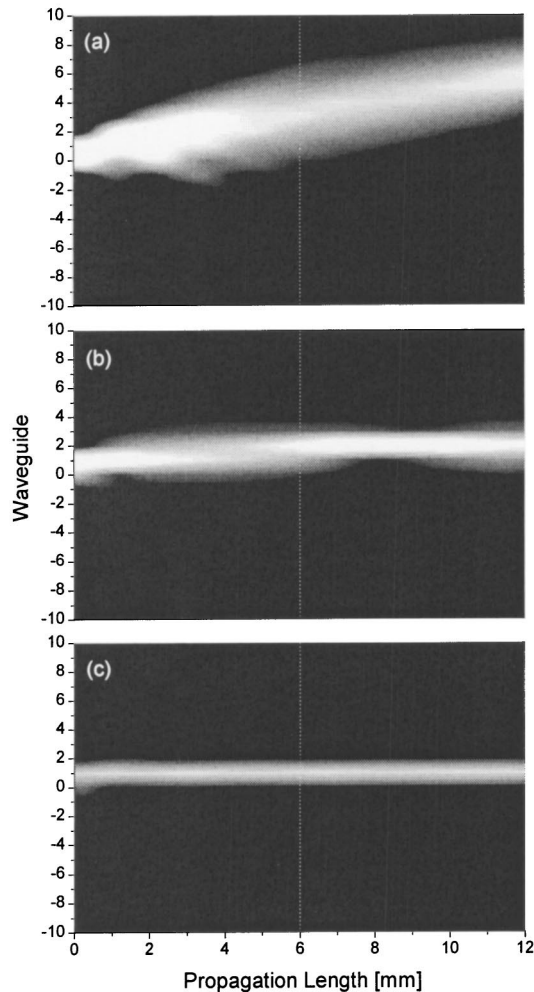


Fig. 11. Simulation based on the DNLS equation [see Eq. (1)] of the field propagation of a displaced beam for different power levels ($9\text{-}\mu\text{m}$ beam size; dashed line, sample length; input position, 0.7 waveguide spacing): (a) 700-W power, (b) 850-W power, (c) 1000-W power.

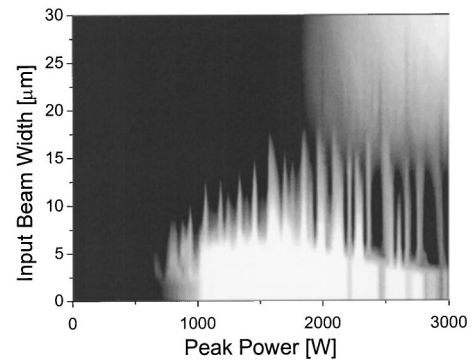


Fig. 12. Simulations of the position-dependent steering based on a complete set of equations [see Eq. (3)]. The entire distance between two waveguides was scanned with the input beam, and the maximum displacement of the first momentum of the power distribution is represented in the graph. Bright areas denote high displacement. The horizontal scale shows incoupled power for the beam centered on a waveguide whereas the vertical scale represents the beam width in terms of FWHM of the input beam. The propagation length is $6\ \text{mm}$.

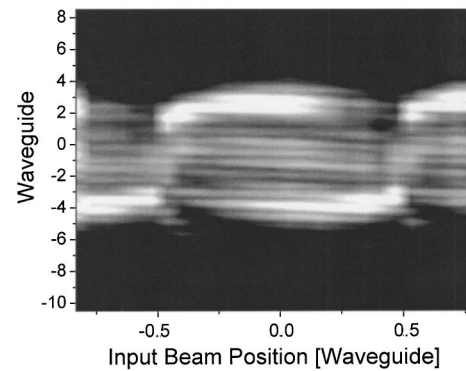


Fig. 13. Output field profiles versus input position if beam breakup occurs ($20\text{-}\mu\text{m}$ beam size, 2000-W peak power).

be achieved by means of an additional weak signal pulse to enable the steering of a discrete soliton into a desired direction.

5. CONCLUSIONS

In conclusion, we have experimentally investigated the dynamic properties of discrete solitons in nonlinear waveguide arrays. Two sets of experiments were performed. We found that, under certain conditions, an initially moving soliton can be captured at the input waveguide, if a certain power is reached. However, once the geometry of the array is fixed, the beam size is of paramount importance. A narrow beam (overlapping approximately two waveguides) could be locked over a relatively significant range (approximately between -0.5° and $+0.5^\circ$), which almost halved for an increment of 50% in soliton size and finally disappeared in the case of a broad beam ($20\ \mu\text{m}$ FWHM).

We also demonstrated that injecting a discrete soliton slightly decentered from a symmetric position leads to significant motion across the array. This phenomenon depends strongly on the beam size. Small displacement of the input position can be amplified up to a factor of 10

for a narrow soliton that propagates in our sample. An increment of 50% in the beam size reduces this lateral motion approximately three times and, finally, a fundamental broad soliton (approximately two times broader than the initial narrow soliton) exhibits the dynamic properties of its continuous counterpart. However, power-induced splitting introduces new effects. For small translations around the equilibrium position, all the power is transferred to one of the two beams, which is emitted with a large lateral velocity. The amplification of a small displacement is even more significant than the one observed for a narrow soliton. All these dynamic properties are extremely fast and power dependent and are potentially useful for all-optical interconnecting and switching.

The authors acknowledge the Israeli Ministry of Science, the British Engineering and Physical Science Research Council (EPSRC), and the Deutsche Forschungsgemeinschaft (German Research Foundation) for their financial support of this research.

*Permanent address, Physikalisches-Astronomische Fakultät, Friedrich-Schiller-Universität Jena, Jena 07743, Germany. U. Peschel's e-mail address is p6peul@rz.uni.jena.de.

†Permanent address, Department of Electrical and Computer Engineering, University of Toronto, 10 King's College Road, Toronto, Ontario M5S 3G4, Canada.

REFERENCES

1. A. Barthelemy, S. Maneuf, and C. Froely, "Propagation soliton et auto-confinement de faisceaux laser par nonlinéarité optique de Kerr," *Opt. Commun.* **55**, 201–206 (1985).
2. J. S. Aitchison, Y. Silberberg, A. M. Weiner, D. E. Leaird, M. K. Oliver, J. L. Jackel, E. M. Vogel, and P. W. E. Smith, "Spatial optical solitons in planar glass waveguides," *J. Opt. Soc. Am. B* **8**, 1290–1295 (1990).
3. D. N. Christodoulides and R. I. Joseph, "Discrete self-focusing in nonlinear arrays of coupled waveguides," *Opt. Lett.* **13**, 794–796 (1988).
4. H. S. Eisenberg, Y. Silberberg, R. Morandotti, A. Boyd, and J. S. Aitchison, "Discrete spatial optical solitons in waveguide arrays," *Phys. Rev. Lett.* **81**, 3383–3386 (1998).
5. S. Flach and C. R. Willis, "Discrete breathers," *Phys. Rep.* **295**, 182–264 (1998).
6. W. Krolikowski, U. Trutschel, M. Cronin-Golomb, and C. Schmitt-Hattenberger, "Solitonlike optical switching in a circular fiber array," *Opt. Lett.* **19**, 320–322 (1994).
7. A. B. Aceves, C. De Angelis, S. Trillo, and S. Wabnitz, "Storage and steering of self-trapped discrete solitons in nonlinear waveguide arrays," *Opt. Lett.* **19**, 332–334 (1994).
8. A. B. Aceves, C. De Angelis, T. Peschel, R. Muschall, F. Lederer, S. Trillo, and S. Wabnitz, "Discrete self-trapping, soliton interactions, and beam steering in nonlinear waveguide arrays," *Phys. Rev. E* **53**, 1172–1189 (1996).
9. R. Morandotti, U. Peschel, J. S. Aitchison, H. S. Eisenberg, and Y. Silberberg, "Dynamics of discrete solitons in optical waveguide arrays," *Phys. Rev. Lett.* **83**, 2726–2729 (1999).
10. A. Yariv, *Optical Electronics*, 4th ed. (Saunders, Philadelphia, Pa., 1991), pp. 519–524.
11. A. Jones, "Coupling of optical fibers and scattering in fibers," *J. Opt. Soc. Am. B* **55**, 261–267 (1965).
12. S. Somekh, E. Garmire, A. Yariv, H. L. Garvin, and R. G. Hunsperger, "Channel optical waveguide directional coupler," *Appl. Phys. Lett.* **22**, 46–48 (1973).
13. H. S. Eisenberg, Y. Silberberg, R. Morandotti, and J. S. Aitchison, "Diffraction management," *Phys. Rev. Lett.* **85**, 1863–1866 (2000).
14. T. Pertsch, T. Zentgraf, U. Peschel, A. Bräuer, and F. Lederer, "Anomalous refraction and diffraction in discrete optical systems," *Phys. Rev. Lett.* **88**, 093901 1–4 (2002).
15. V. E. Zakharov and A. B. Shabat, "Exact theory of two-dimensional self focusing and one-dimensional self modulation of waves in nonlinear media," *Sov. Phys. JETP* **34**, 62–69 (1972).
16. Y. S. Kivshar, "Self-localization in arrays of defocusing waveguides," *Opt. Lett.* **18**, 1147–1149 (1993).
17. J. S. Aitchison, D. C. Hutchings, J. U. Kang, G. I. Stegeman, and A. Villeneuve, "The nonlinear optical properties of AlGaAs at the half band gap," *IEEE J. Quantum Electron.* **33**, 341–348 (1997).
18. Y. V. Afanasjev, J. S. Aitchison, and Y. S. Kivshar, "Splitting of high-order spatial solitons under the action of 2-photon absorption," *Opt. Commun.* **116**, 331–338 (1995).
19. Y. Silberberg, "Solitons and two-photon absorption," *Opt. Lett.* **15**, 1005–1007 (1990).